ACS Partner Journal

ENVIRONMENT & HEALTH

Open Access

pubs.acs.org/EnvHealth

Article

Impact of 4-*tert*-Butylphenol on Inflammation and Glycogen Metabolism in *Cyprinus carpio* L via the miR-363/PKCδ Axis

Jiawen Cui, Xinchi Shang, Yuhao Liu, Xiaohua Teng, Li Zhou,* and Bing Yan

Cite This: *Environ. Health* 2025, 3, 539−550

Read Online

ACCESS | Metrics & More | Article Recommendations | Supporting Information

ABSTRACT: 4-*tert*-Butylphenol (4-tBP), widely used in manufacturing polycarbonate plastics and epoxy resins, is commonly found in aquatic environments globally. This study investigates the chronic (60 days) hepatotoxic effects and the underlying mechanism of 4-tBP on fish, including concentrations with environmental relevance (≤100 μg/L), using *Cyprinus carpio* L. as the model. Results showed that 1−500 μg/L 4-tBP triggered significant alterations in oxidative stress markers (superoxide dismutase (SOD), glutathione peroxidase (GPx), and malondialdehyde (MDA)) and liver enzymes (alanine aminotransferase (ALT) and aspartate aminotransferase (AST)), with a dose−response relationship confirmed by the Integrated Biomarker Response (IBR) index. Histopathological analysis and molecular experiments revealed inflammatory responses, disruptions in glycogen metabolism, and critical insulin signaling pathways (IRS1, AKT, and GSK3β). Further investigations, including miRNA sequencing and *in vitro* assays in primary hepatocytes, identified the miR-363/PKCδ axis as a critical regulatory pathway affecting these changes. This study demonstrated that chronic, low-level exposure to 4-tBP can induce hepatotoxicity in *Cyprinus carpio* L. via the miR-363/PKCδ axis. These findings highlight the potential ecological and health risks posed by 4-tBP in the environment and suggest potential targets for therapeutic intervention.

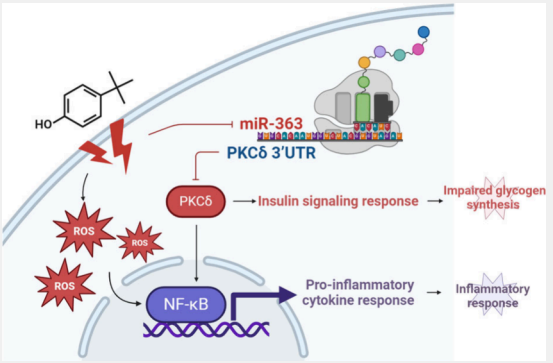

KEYWORDS: *4-tert-Butylphenol, Integrated Biomarker Response, Inflammation, Glycogen Metabolism, miR-363/PKCδ Axis*

1. INTRODUCTION

Endocrine-disrupting chemicals (EDCs) are a growing concern due to their widespread presence in the environment and their ability to interfere with the endocrine systems of both wildlife and humans. One such EDC, 4-*tert*-butylphenol (4-tBP), is widely used in manufacturing polycarbonate plastics, epoxy resins, cleaning agents, and other industrial materials.[1,2] A study has found high levels of 4-tBP in consumer products such as paints and adhesives, with concentrations reaching up to 320 g/kg.[1] These products and industrial wastewater discharge can quickly release 4-tBP into the environment, leading to its accumulation.[3,4] Environmental monitoring has detected 4-tBP in diverse aquatic settings, with concentrations ranging from 0.225 to 1.121 μg/L in the Nanjing section of the Yangtze River in China[5] and varying from 0.003 to 64 μg/L in leachates from Japanese municipal solid waste sites.[6] Notably, sewage treatment plants in Korea have reported levels up to 218.2 μg/L.[7] The multiple sources and widespread occurrences of 4-tBP in the environment highlight the importance of understanding the risks posed by 4-tBP to both ecological systems and human health.

Research has shown that 4-tBP exhibited non-negligible intrinsic acute toxicity, with a 96 h-LC_{50} value of 5.1 mg/L for *Pimephales promelas* (fathead minnow), as reported by the Environmental Agency of Japan.[8] Multiple types of ecotoxicological problems, including genotoxicity and reproductive toxicity, have been observed upon 4-tBP exposure. For example, exposure to 4-tBP at 100 mg/L increased prenatal testosterone and progesterone levels in rats.[9] In *Danio rerio* (zebrafish), parental exposure to 4-tBP at concentrations of 4 μmol/L (equivalent to 600.88 μg/L) hindered the growth and development of F1 embryos[10] and interfered with critical lipid metabolism pathways.[10,11] Additionally, 4-tBP has been found to disturb metabolic processes and induce inflammation in *Cyprinus carpio* L. (common carp) at exposure levels up to 690 μg/L, although no behavioral changes were observed.[12] However, most existing studies of 4-tBP toxicity have focused on acute or short-term effects at concentrations that are much higher than those found in aquatic environments. The potential adverse effects of chronic exposure to 4-tBP at environmentally relevant levels have been poorly characterized.

The liver, a primary organ for the uptake and metabolism of foreign chemicals, is particularly vulnerable to 4-tBP. As a

Received: November 15, 2024
Revised: February 3, 2025
Accepted: February 6, 2025
Published: February 13, 2025

https://doi.org/10.1021/envhealth.4c00242
Environ. Health 2025, 3, 539−550

lipophilic contaminant, 4-tBP can enter the body and accumulate in the liver.[13] A study by Sundt et al. observed a positive correlation between liver 4-tBP content and oral exposure in *Gadus morhua* (Atlantic cod).[14] In addition, impaired glucose metabolism, structural damage to liver cells, and elevated oxidative stress were found in aquatic species exposed to 4-tBP concentrations up to 600 μg/L.[10] Recent findings suggest that 4-tBP further impairs liver function by inducing excess lipid accumulation and peroxidation, as well as disrupting the lipid metabolism pathway.[10,15] Although the liver has been demonstrated to be the primary target for 4-tBP toxicity, the mechanisms behind these pathological effects remain to be elucidated.

This study explores the potential hepatotoxic effects and the underlying mechanism of long-term exposure to environmentally relevant levels of 4-tBP, employing *Cyprinus carpio* L., a model widely used in aquatic toxicology research.[16] *Cyprinus carpio* L. was exposed to 4-tBP for 60 days, with concentrations of 1, 10, and 100 μg/L that were in line with the levels typically found in environmental water. Hepatotoxicity was evaluated through an Integrated Biomarker Response (IBR) index calculated from oxidative stress markers, histopathological analyses, and molecular approaches. The mechanism underlying the effect of 4-tBP was determined via miRNA sequencing and *in vitro* assays and further validated by target mRNA silencing assays. These comprehensive toxicological assessments could advance our understanding of the potential risks of environmental 4-tBP and help identify therapeutic targets for mitigating its harmful effects.

2. MATERIALS AND METHODS

2.1. Fish Culture and Treatment

A total of 135 healthy *Cyprinus carpio* L. (66.42 ± 5.37 g) were domesticated in 260 L aquariums. The fish were exposed to 4-tBP at 1, 10, 100, and 500 μg/L. The selected concentrations were based on the reported environmental levels of 4-tBP in various aquatic systems. A concentration of 1 μg/L represents levels detected in some natural water bodies, such as the Nanjing section of the Yangtze River (0.225−1.121 μg/L[5]). The 10 μg/L concentration reflects conditions in moderately polluted environments, while 100 μg/L corresponds to levels near heavily contaminated sites, such as 64 μg/L in Japanese landfill leachates[6] and 218.2 μg/L in Korean sewage treatment plants.[7] The highest concentration (500 μg/L), although exceeding typical environmental levels, was included to simulate extreme contamination and to investigate dose−response relationships. Measured 4-tBP concentrations were 0.77 ± 0.16, 7.62 ± 1.18, 73.03 ± 16.04, and 423.25 ± 45.61 μg/L, corresponding to nominal levels of 1, 10, 100, and 500 μg/L, respectively. After 60 days, blood and liver samples were collected. The study was approved by the Animal Protection Institution and Use Committee of Northeast Agricultural University (approval number: NEAUEC20210211). More details are provided in Text S1.

2.2. Serum Biochemistry Determination

The serum was separated from collected blood samples by centrifugation at 4,000*g* for 5 min. The enzymatic activities of alanine aminotransferase (ALT) and aspartate aminotransferase (AST) were quantified using commercial assay kits supplied by Reebio Biotechnology Co., Ltd. (Ningbo, China), following the manufacturer's protocol. Absorbance changes at 340 nm, indicative of enzyme activity, were monitored by using a TBA-2000FR automatic biochemical analyzer (Toshiba Corporation, Tokyo, Japan).

2.3. Oxidative Stress Biomarkers Assay

The liver samples (0.1 g) were homogenized in 0.9 mL of 0.86% saline solution using a motor-driven tissue grinder (Model D-160, Beijing Dalong Xingchuang Experimental Instrument Co., Ltd., China). The homogenate was centrifuged at 4 °C and 1,000*g* for 15 min to separate the supernatant. The collected supernatant was used to assess oxidative stress biomarkers, including superoxide dismutase (SOD), glutathione peroxidase (GPx), and malondialdehyde (MDA), using assay kits provided by Nanjing Jiancheng Bioengineering Institute Co., Ltd., Nanjing, China. All procedures followed the manufacturer's instructions to ensure accuracy and consistency in the assay results.

2.4. Integrated Biomarker Response (IBR) Analysis

IBR, an integrated multibiomarker response index, was selected to assess the ecological risk posed by 4-tBP to *Cyprinus carpio* L.[17,18] Five biochemical indicators (SOD, GPx, MDA, ALT, and AST) were selected for the IBR calculation. The calculation method was adopted from a previous study,[19] and the steps involved are as follows:

$$Y_i = \log\left(\frac{X_i}{X_0}\right) \tag{1}$$

where Y_i is the normalized value of different biomarkers in each group, X_i is the average value of the biomarkers in the treatment groups, and X_0 is the average value of the biomarkers in the control group.

$$Z_i = (Y_i - \mu)/\sigma \tag{2}$$

where Z_i is the normalized value of the biomarker in each group, μ is the average value of Y_i, and σ is the standard deviation of Y_i.

$$A_i = Z_i - Z_0 \tag{3}$$

where A_i is the deviation index of the biomarker ($A > 0$ represents activation; $A < 0$ represents inhibition); Z_0 is the normalized value of the biomarker in the control group.

$$\mathrm{IBR} = \sum |A_i| \tag{4}$$

where the IBR value represents the sum of the absolute values of the deviation index for all biomarkers.

2.5. Hematoxylin-Eosin (H&E) Staining

The liver tissue samples, measuring 1−2 cm^3, were first fixed in 4% paraformaldehyde. Following fixation, tissues were progressively dehydrated through an ethanol series and embedded in paraffin wax. Thin sections of 5−6 μm were then prepared using a microtome. These sections were stained with hematoxylin and eosin (H&E) to highlight cellular and structural details, facilitating the examination of histopathological alterations. The stained sections were subsequently observed under a confocal microscope (NIS-Elements 5.4, Nikon, Japan) for detailed tissue analyses.

2.6. Transmission Electron Microscopy (TEM) Observation

The liver tissue samples (0.5−1 mm^3) were initially fixed in 2.5% glutaraldehyde, postfixed in osmium tetroxide, dehydrated through a graded series of ethanol solutions, and embedded in epoxy resin. Ultrathin sections (50−60 nm) were prepared using an ultramicrotome and then stained with uranyl acetate and lead citrate to enhance contrast. These sections were examined using an H7650 transmission electron microscope (TEM, HITACHI, Tokyo, Japan) to observe the ultrastructural changes within the liver tissue.

2.7. MiRNA-Sequencing and Target-Gene Prediction

MiRNA sequencing of *Cyprinus carpio* L. liver tissues was performed after RNA extraction and small RNA library preparation. Q-PCR validated the libraries, and sequencing was done on an Illumina HiSeq 3000 system. Reads were processed, collapsed, and aligned with the Rfam database to isolate miRNAs. Differential miRNA expression ($|\log_2\mathrm{FoldChange}| > 1$ and $P\text{-adj} < 0.05$) was analyzed, and target genes were predicted using the miRanda platform. More details are given in Text S2.

https://doi.org/10.1021/envhealth.4c00242
Environ. Health 2025, 3, 539−550

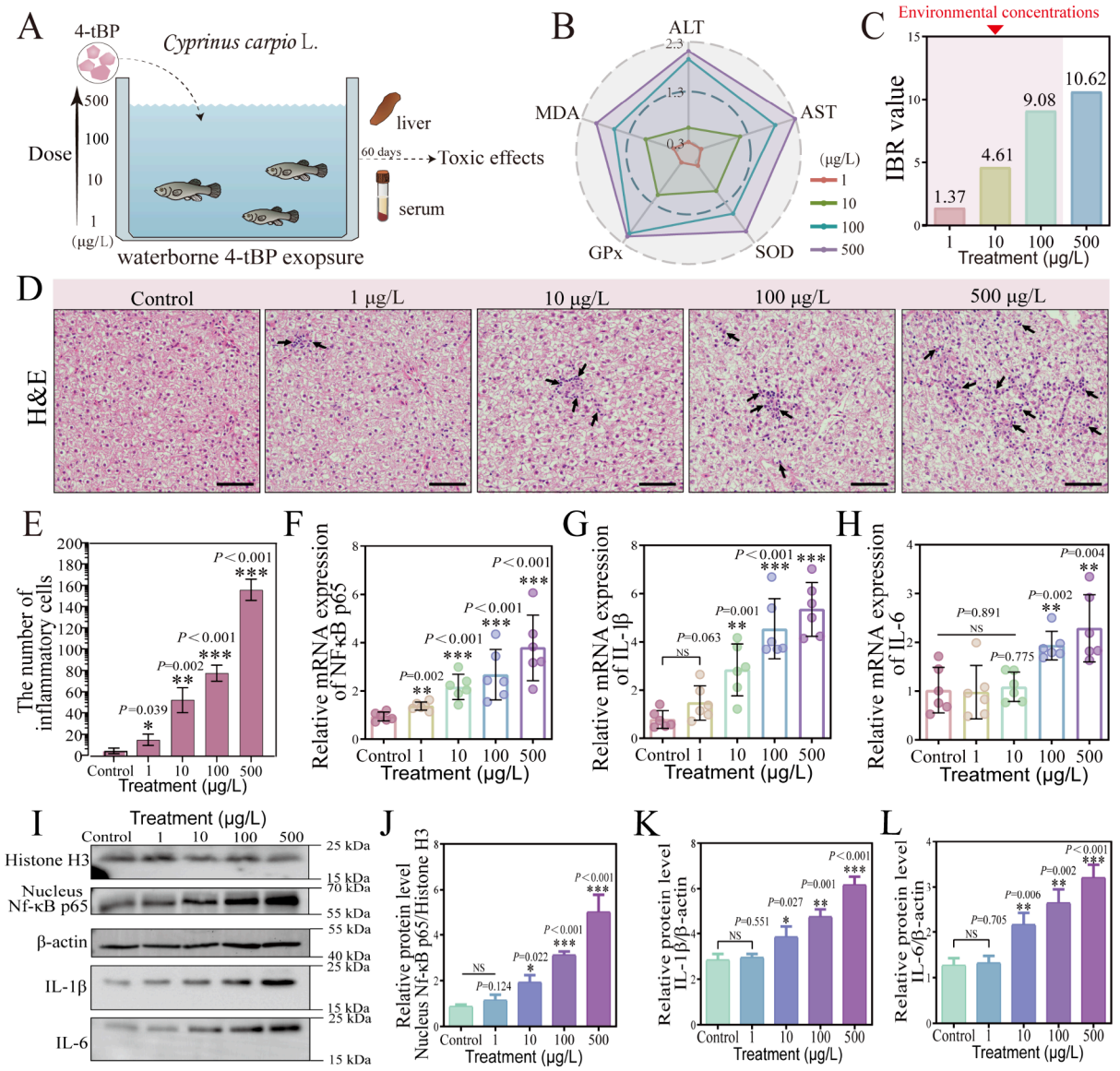

Figure 1. 4-tBP exposure induced dose-dependent inflammatory response in *Cyprinus carpio* L. livers under 60-day exposure. (A) Schematic of the exposure experiments. (B) Radar plots for the IBR of multiple biomarkers of liver damage after exposure to varying concentrations of 4-tBP. (C) IBR values at different exposure concentrations of 4-tBP. (D) H&E images displaying hepatic ultrastructure. Scale bars: 50 μm. The arrow points to inflammatory cell infiltration. (E) Quantification of inflammatory cells per field (n = 3). (F–H) Relative mRNA levels of NF-κB p65, IL-1β, and IL-6 in liver tissues treated with varying concentrations of 4-tBP using the qRT-PCR assay. (I) Western blot assay presenting the protein levels of nuclear NF-κB p65, IL-1β, and IL-6. (J–L) Densitometric analysis of Western blot bands (n = 3).

2.8. Isolation and Culture of Primary Hepatocytes of *Cyprinus carpio* L

Isolation and culture of primary hepatocytes from *Cyprinus carpio* L. were performed as previously described.[15] The fish were treated with potassium permanganate and anesthetized, and the liver tissue was aseptically collected. The tissue was washed, cut into small pieces, and digested with trypsin. Hepatocytes were isolated and cultured at 28 °C. For an overview of the protocols used for cell isolation and culture, please refer to Text S3.

2.9. Establishment of miR-363 Mimic/Inhibition and siRNA PKCδ Model in Hepatocytes

Transfection reagents (miR-363 mimic/inhibitor, NC controls, siRNA PKCδ, and siNC) were synthesized by Guangzhou RiboBio Co., Ltd., with concentrations validated by qRT-PCR (Figure S1; sequences are in Table S1). Transfection was performed using 2 μL of Lipofectamine 2000 in 1 mL of Opti-MEM, followed by a 6 h cotransfection and 24 h incubation with or without 100 μmol/L 4-tBP (details in Table S2). For a comprehensive understanding of the methods employed, please refer to Text S4.

2.10. Periodic Acid Schiff (PAS) Staining

PAS staining was conducted to evaluate the effects of 4-tBP and miR-363 on the hepatic glycogen synthesis. Fixed liver tissues and treated hepatocytes were stained and imaged by using confocal and fluorescence microscopes, respectively. Glycogen intensity was quantified with ImageJ. Methods for the analysis are given in Text S5.

2.11. Plasmids Construction and Dual-Luciferase Reporter Assay

Plasmid construction and dual-luciferase reporter assays were performed using the pmiR-RB-REPORT vector. The 3′ untranslated region (3′ UTR) sequences of wild-type (PKCδ-WT) and mutant PKCδ (PKCδ-MUT) were inserted into the vector, with sequences provided in Table S3. The plasmids were cotransfected with NC-M and miR-363 mimic into cells using Lipofectamine 6000. Luciferase activity was measured with the Dual-Luciferase Reporter Assay

https://doi.org/10.1021/envhealth.4c00242
Environ. Health 2025, 3, 539−550

System, normalized to that of Firefly Luciferase. More details are presented in Text S6.

2.12. qRT-PCR Analysis

The qRT-PCR experiment was conducted following a recent report from our laboratory.[20] Total RNA was extracted from liver tissues and primary hepatocytes with a Trizol reagent (Invitrogen, Carlsbad, California, USA). After cDNA synthesis, PCR amplification was performed using the LightCycler480 Real-Time PCR system (Roche, Basel, Switzerland). The specific primers were synthesized by Sangon Biotech Co., Ltd. (Shanghai, China), and primer sequences are shown in Table S4. β-Actin was used as the internal reference gene for mRNA, while U6 was used as the internal reference gene for miRNAs. Relative RNA expression levels were calculated using the $2^{-\Delta\Delta Ct}$ method.

2.13. Western Blot Assay

Total and nuclear proteins were exacted, quantified, subjected to SDS-PAGE, and then transferred to nitrocellulose membranes. After blocking, membranes were incubated overnight at 4 °C with primary antibodies (Table S5) and then with HRP-conjugated secondary antibodies. Detection was performed using BeyoECL Star. β-Actin and Histone H3 were internal references for the total and nuclear proteins. Protein expression levels were calculated as the target protein's optical density ratio to the internal reference. For detailed methods, please refer to Text S7.

2.14. Statistical Analysis

IBM SPSS Statistics 23.0 (Chicago, IL, USA) was used for statistical analysis. All data were tested for normal distribution using the Shapiro−Wilk method. Independent sample t tests and one-way or two-way ANOVA with Tukey's multiple comparison tests were performed, and the data were expressed as the mean ± standard deviation (SD). Different letters and * represented significant differences ($P < 0.05$), and the same letter and NS represented nonsignificant difference ($P \geq 0.05$). * means $P < 0.05$, ** means $P < 0.01$, and *** means $P < 0.001$.

3. RESULTS AND DISCUSSION

3.1. Dose-Dependent Hepatotoxicity of 4-tBP in *Cyprinus carpio* L

The potential toxicity of 4-tBP to aquatic organisms at environmentally relevant levels has garnered widespread concern. In this study, *Cyprinus carpio* L. was exposed to 4-tBP across a gradient of concentrations over a period of 60 days (Figure 1A). Previous studies have revealed that 4-tBP primarily accumulates in the liver, inducing an array of hepatic physiological responses, with oxidative stress frequently cited as a predominant manifestation.[13,15] The activity of antioxidant enzymes is recognized as an early biomarker of oxidative stress.[21] Our observations (Figure S2A,B) showed a dose-responsive decrement in the activities of pivotal hepatic antioxidant enzymes (SOD and GPx) with increasing 4-tBP concentrations. At the lowest concentration (1 μg/L), SOD activity showed no statistically significant change compared to the control (47.2 ± 16.2 U/mg of prot vs. 56.9 ± 16.7 U/mg prot, $P = 0.161$), while GPx activity decreased significantly by 13.1% ($P = 0.044$). At higher concentrations, the decline in enzyme activity became more pronounced. For instance, at 100 μg/L, the activities of SOD and GPx ($P < 0.001$) decreased by 59.6% and 70.2%, respectively. These findings suggest that long-term exposure to even low levels of 4-tBP impairs the liver's antioxidant defenses. This impairment diminishes the liver's ability to neutralize reactive oxygen species (ROS) and increases the risk of lipid peroxidation through free radical chain reactions.[22] Consistent with these observations, hepatic H_2O_2 levels (Figure S2C) increased significantly by 41.5%, 193.6%, and 281.9% at 10, 100, and 500 μg/L of 4-tBP exposure, respectively. However, no significant changes were observed at 1 μg/L ($P = 0.890$) and 10 μg/L ($P = 0.214$). The increase of MDA levels (Figure S2D), an indicator of oxidative stress that can induce cellular to tissue-level damage, further corroborated the dose-dependent effect of 4-tBP on lipid peroxidation.[23] Additionally, serum ALT and AST levels, reliable biomarkers for liver dysfunction,[24] showed a dose-dependent activity increase (Figure S3). Significant elevations were observed at concentrations of 10 μg/L and higher, with ALT levels increasing by 27.9% ($P = 0.006$) and AST levels, by 80.7% ($P < 0.001$) at 10 μg/L of 4-tBP. These results highlight progressive liver damage associated with increasing 4-tBP exposure, demonstrating its hepatotoxic effects even at environmentally relevant concentrations.

The IBR method was applied in this study to quantitatively assess the hepatotoxic effects by integrating multiple biomarker responses.[17,25] In our study, we normalized and visualized the response levels of five biomarkers (SOD, GPx, MDA, ALT, and AST) across a gradient of 4-tBP concentrations. As depicted in Figure 1B, the progressive expansion of the profile area with increasing 4-tBP concentrations illustrated the cumulative stress response dictated by dose-dependency. The IBR value at the lowest 4-tBP concentration (1 μg/L) was 1.37 (Figure 1C), indicating an adaptive response with minimal hepatic damage. However, at 10 μg/L, the IBR value tripled to 4.61, signifying a challenge to adaptive mechanisms and a decline in hepatic health. At higher concentrations of 4-tBP (100 and 500 μg/L), the IBR values increased sharply to 9.08 and 10.62, respectively, suggesting an overburdened hepatic detoxification system, increased oxidative stress, and potential cellular damage. The gradual increase in IBR values clearly demonstrated the dose-dependent hepatotoxicity of 4-tBP in *Cyprinus carpio* L. Recent studies supported our conclusion regarding the dose−response toxicity of EDCs on aquatic animals through IBR analysis.[26,27] For example, Yang et al. found that multiple oxidative stress biomarkers (including SOD, catalase, ROS, and MDA) in *Procambarus clarkii* responded to atrazine exposure, with IBR analysis confirming its dose-dependent toxicity on crayfish.[27] Similarly, Briaudeau et al. demonstrated a dose-dependent hepatotoxicity of polycyclic aromatic hydrocarbons in Senegalese sole juveniles, as evidenced by increasing IBR values with rising exposure concentrations.[26] Therefore, our findings suggest the potential health risks of 4-tBP to aquatic ecosystems.

3.2. Inflammation Mediated by the NF-κB Pathway in Response to 4-tBP Exposure

We conducted histopathological analyses on liver tissues to visually assess the liver damage induced by 4-tBP. H&E staining results (Figure 1D) showed normal liver morphology in the control, with no significant signs of inflammatory infiltration. However, a progressive accumulation of inflammatory cells (indicated by arrows) was observed with increasing concentrations of 4-tBP, indicating an ongoing inflammatory response. Quantitative analysis (Figure 1E) confirmed a significant increase in inflammatory cells, rising from 5.0 ± 2.6 cells/field in the control to 15.7 ± 5.5 cells/field at 1 μg/L ($P = 0.039$) and further to 78.3 ± 7.5 cells/field at 100 μg/L ($P < 0.001$). This inflammatory response is likely associated with oxidative stress induced by 4-tBP. Oxidative stress typically precedes and contributes to initiating and perpetuating inflammatory cascades.[28] It activates the Nuclear Factor-

https://doi.org/10.1021/envhealth.4c00242
Environ. Health 2025, 3, 539−550

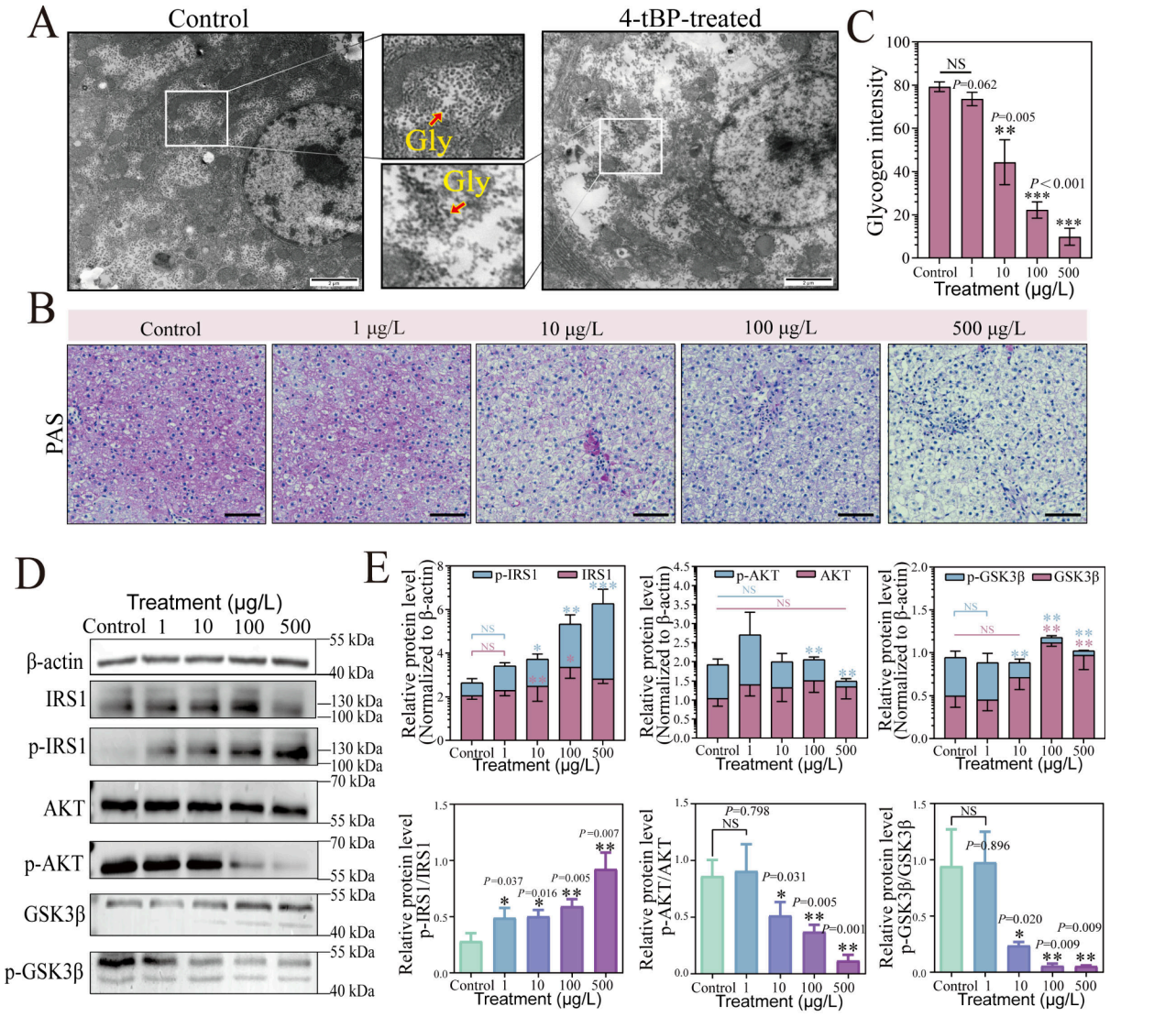

Figure 2. 4-tBP disrupted hepatic glycogen metabolism in *Cyprinus carpio* L. under 60-day exposure. (A) TEM images displaying hepatic ultrastructure in control and 4-tBP-treated *Cyprinus carpio* L. Scale bars: 2 μm. The middle panels represent magnified views of the white boxed areas in the corresponding TEM images. The arrow points to glycogen (Gly). (B) PAS staining of liver tissues. Scale bars: 50 μm. (C) Quantification of PAS staining using ImageJ. (D) Western blot assay presenting the protein levels of β-actin, IRS1, p-IRS1 Ser-307, AKT, p-AKT Ser-473, GSK3β, and p-GSK3β Ser-9 in both control and 4-tBP-treated groups. (E) Densitometric analysis of Western blot bands (n = 3).

kappa B (NF-κB) pathway, a central regulator of inflammatory responses frequently triggered by oxidative stress and environmental toxicants.[29,30] Oxidative stress activates the NF-κB pathway, leading to upregulation of pro-inflammatory cytokines Interleukin-1 beta (IL-1β) and Interleukin-6 (IL-6). This promotes immune cell recruitment and activation in damaged tissues.[31] We evaluated mRNA expression levels of key pro-inflammatory markers (NF-κB p65, IL-1β, and IL-6) to unravel the molecular mechanisms underlying the observed histopathological changes. NF-κB p65 mRNA expression increased dose-dependently, with significant upregulation observed at 1 μg/L (1.46-fold, P = 0.002) and peaking at 100 μg/L (2.9-fold, P < 0.001) compared to the control (Figure 1F). Similarly, IL-1β and IL-6 mRNA levels showed significant increases, reaching 5.8-fold (P < 0.001) and 2.4-fold (P = 0.002) at 100 μg/L, respectively (Figure 1G,H). Consistent with the mRNA data, Western blot results (Figure 1I–L, Uncropped Western blots for Figure S6) showed an increase in protein levels of nuclear NF-κB p65 at higher treatment concentrations, which is a hallmark of NF-κB p65 activation and nuclear translocation.[32] This critical translocation facilitates the transcriptional activation of numerous inflammatory genes, including IL-1β and IL-6.[33,34] The increase in the IL-1β and IL-6 protein levels aligns with their mRNA trends, suggesting a pronounced NF-κB-mediated inflammatory cascade in response to 4-tBP exposure. These results align with studies on other alkylphenols, which have been shown to activate NF-κB signaling, further amplifying inflammatory responses.[35,36] Notably, our results are consistent with findings from recent studies showing that 4-tBP can induce pro-inflammatory responses across diverse cell types and species.[37,38] For instance, 4-tBP exposure has been shown to elevate IL-6 expression in human melanocytes.[37] This cross-species consistency underscores the pro-inflammatory potential of 4-tBP, highlighting its relevance as an environmental risk factor.

https://doi.org/10.1021/envhealth.4c00242
Environ. Health 2025, 3, 539−550

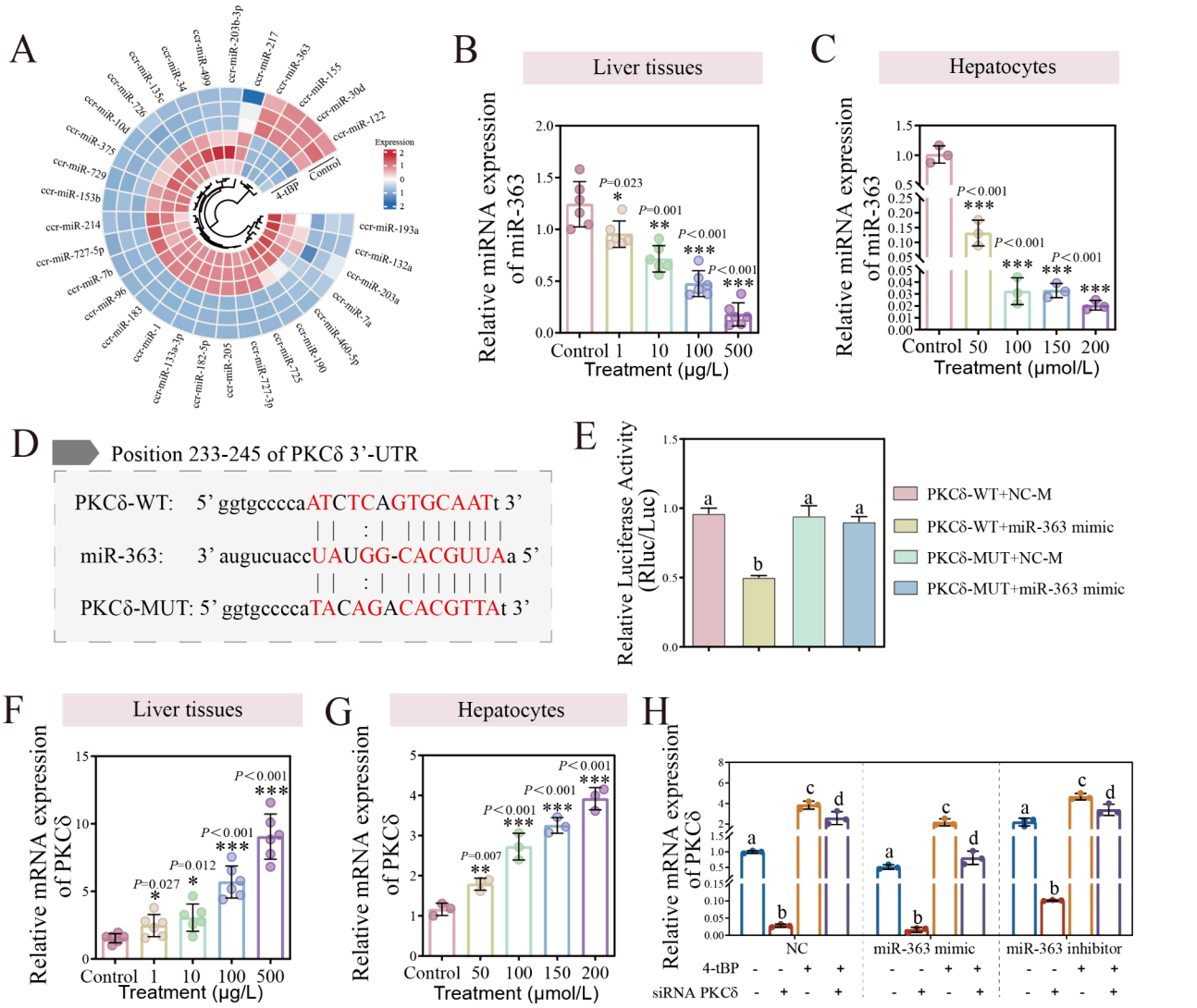

Figure 3. Presence of MiR-363/PKCδ axis under 4-tBP exposure. (A) Circular heatmap representation of differentially expressed miRNAs in liver tissue following 4-tBP treatment (500 μg/L) (n = 3). (B) Relative miR-363 expression level in liver tissues using qRT-PCR (n = 6). (C) Relative miR-363 expression level in primary hepatocytes of *Cyprinus carpio* L. using qRT-PCR (n = 3). (D) Alignment of miR-363 with the 3′ UTR of both the wild-type (PKCδ-WT) and mutant-type (PKCδ-MUT) of PKCδ at the predicted binding sites. (E) Relative luciferase activity assay results (n = 3). (F) Relative mRNA expression in liver tissues (n = 6). (G) Relative mRNA expression in primary hepatocytes of *Cyprinus carpio* L. (n = 3). (H) Relative mRNA expression in primary hepatocytes of *Cyprinus carpio* L. (n = 3).

3.3. Inflammation-Associated Disruption of Hepatic Glycogen Metabolism

Inflammatory response significantly affects hepatic glycogen metabolism by disrupting key signaling pathways such as the insulin signaling cascade.[39,40] To determine whether disruptions in hepatic glycogen metabolism accompany the inflammation induced by 4-tBP, we analyzed the ultrastructure of liver tissues. TEM observations (Figure 2A) revealed significant ultrastructural changes in hepatocytes exposed to 500 μmol/L 4-tBP, characterized by uneven and sparse glycogen distribution compared to the control's uniform and abundant glycogen stores. This finding was further corroborated by PAS staining (Figure 2B,C), which showed a dose-dependent reduction in glycogen content in livers exposed to 4-tBP. Glycogen levels were significantly reduced by 44.1% at 10 μg/L, 72.0% at 100 μg/L, and 87.6% at 500 μg/L, compared to the control group. These results suggested that long-term 4-tBP exposure disrupted hepatocyte glycogen metabolism, leading to liver damage.

At the molecular level, hepatic glycogen metabolism is stringently regulated by the insulin signaling pathway,[41] which can be affected by the NF-κB-mediated inflammation.[42,43] For instance, NF-κB activation has been demonstrated to inhibit insulin signaling by interfering with IRS1/AKT/GSK3β phosphorylation in HepG2 cells.[40] Our findings (Figure 2D,E, Uncropped Western blots for Figure S6) indicated that the phosphorylation level of IRS1 at Ser-307 increased with increasing concentrations of 4-tBP. Specifically, p-IRS1 levels increased by 2.1-fold at 10 μg/L, 3.4-fold at 100 μg/L, and 5.9-fold at 500 μg/L, compared to the control. The ratio of phosphorylated to total IRS1 (p-IRS1/IRS1) also increased dose-dependently, with significant (P < 0.05) differences observed at all treatments. The phosphorylation of IRS1 at Ser-307 has been recognized as an inhibitory modification,[44] disrupting insulin signaling and contributing to insulin resistance under stress conditions.[45] Previous studies have

https://doi.org/10.1021/envhealth.4c00242
Environ. Health 2025, 3, 539−550

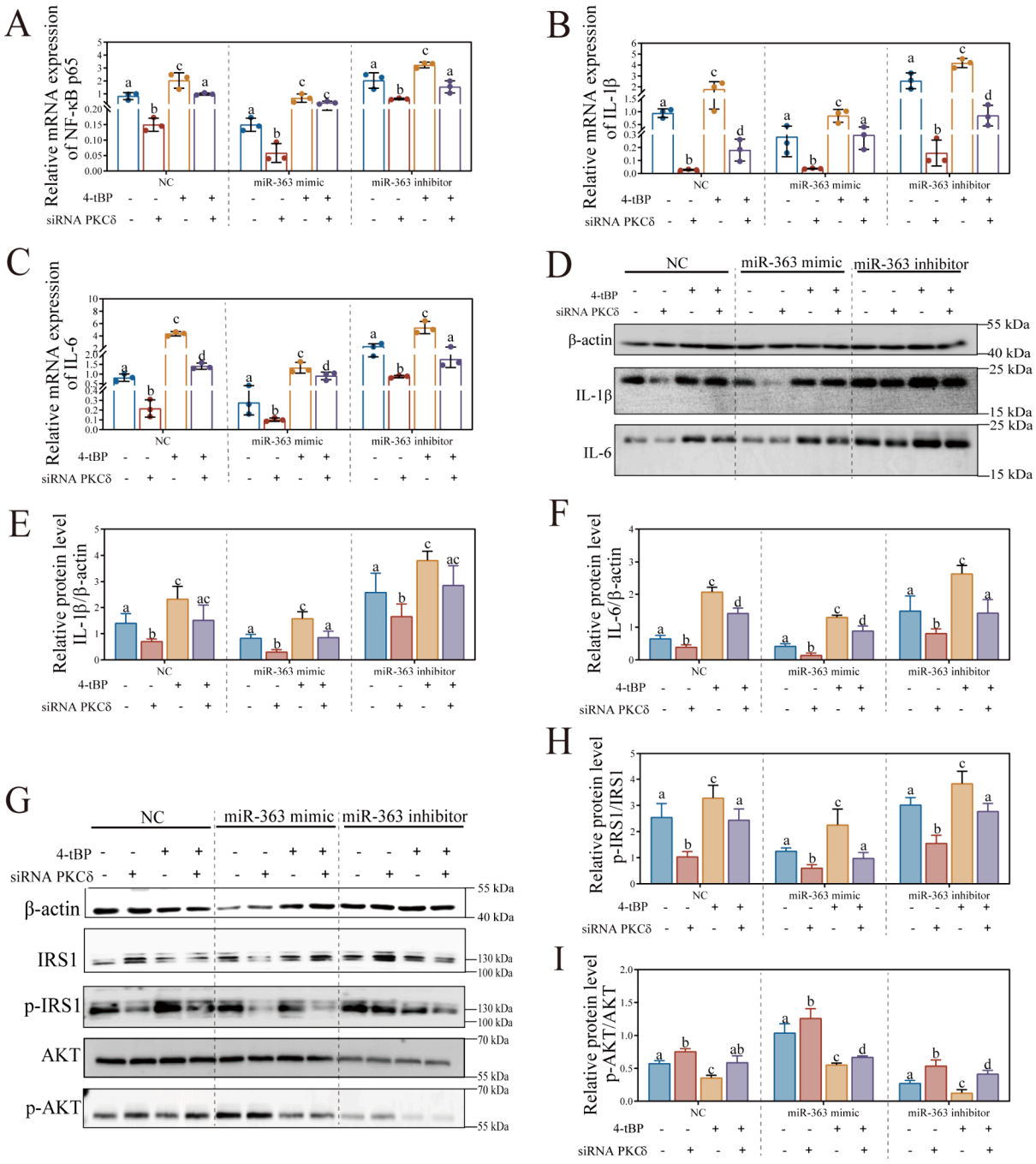

Figure 4. Modulation of inflammatory and insulin signaling pathway by miR-363/PKCδ axis in response to 4-tBP exposure. (A–C) Relative mRNA expression of NF-κB p65, IL-1β, and IL-6 in primary hepatocytes of *Cyprinus carpio* L. (n = 3). (D) Western blot assay presenting the protein levels of β-actin, IL-1β, and IL-6. (E, F) Densitometric analysis of Western blot bands (n = 3). (G) Western blot assay presenting the protein levels of β-actin, IRS1, p-IRS1 Ser-307, AKT, and p-AKT Ser-473. (H–I) Densitometric analysis of Western blot bands (n = 3).

shown that short-term insulin stimulation increases total IRS1 levels, while prolonged stimulation leads to elevated serine phosphorylation of IRS1.[46] This modification promotes IRS1 degradation, resulting in a reduction in total IRS1 levels and disruption of downstream insulin signaling.[46] This mechanism aligns with our observation that total IRS1 levels significantly increased by 21.0% at 10 μg/L and 62.6% at 100 μg/L but plateaued at 500 μg/L with no further significant increase. Subsequently, this reduces in the phosphorylation level of its downstream effector, Protein Kinase B (AKT), at Ser-473.[47] AKT plays an important role in insulin signaling by phosphorylating and inactivating Glycogen Synthase Kinase 3 beta (GSK3β).[48] In our study, a significant (P < 0.05) dose-dependent reduction in the ratios of p-AKT/AKT was observed, dropping by 40.4% at 10 μg/L (P = 0.031), 57.0% at 100 μg/L (P = 0.005), and 86.7% at 500 μg/L (P = 0.001). This reduction impaired the ability of AKT to phosphorylate and inactivate GSK3β, resulting in sustained GSK3β activity and subsequent inhibition of glycogen synthesis.[49] Consistent with this finding, we observed a significant (P < 0.05) dose-dependent decline in the p-GSK3β/GSK3β ratio at 10 μg/L and higher 4-tBP exposure concentrations. Specifically, the p-

https://doi.org/10.1021/envhealth.4c00242
Environ. Health 2025, 3, 539–550

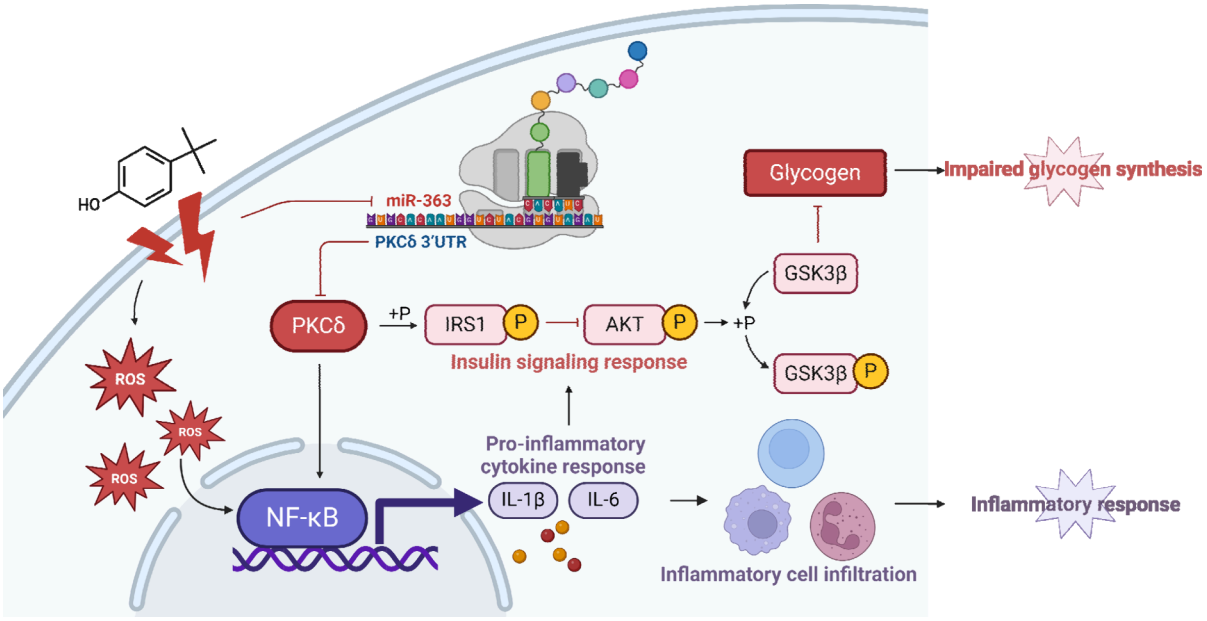

Figure 5. Schematic diagram of the mechanism by which 4-tBP-induced hepatotoxicity. The miR-363/PKCδ axis emerges as a pivotal modulator of 4-tBP-induced inflammation and glycogen synthesis impairment by regulating the NF-κB signaling and insulin signaling pathways.

GSK3β/GSK3β ratio decreased by 74.9% at 10 μg/L, 93.8% at 100 μg/L, and 98.2% at 500 μg/L compared to the control. Additionally, total GSK3β levels showed a notable increase under high 4-tBP concentrations (100 and 500 μg/L), confirming its inhibitory effect on glycogen synthesis. These findings demonstrated that 4-tBP disrupted the insulin signaling pathway in a dose-dependent manner through the IRS1/AKT/GSK3β pathway. Similar disruptions in insulin signaling through the IRS1/AKT/GSK3β pathway have been observed in previous studies on some endocrine-disrupting chemicals, such as bisphenol A and di(2-ethylhexyl) phthalate.[50,51]

3.4. Identifying miR-363 as a Key Regulator in 4-tBP-Induced Hepatotoxicity

Numerous studies have suggested the critical roles of miRNAs in mediating various cellular processes, including inflammatory pathways and metabolic regulations.[52,53] Some miRNAs have been implicated in mediating inflammatory responses and metabolic signaling pathways when exposed to environmental EDCs.[54,55] For instance, exposure to di(2-ethylhexyl) phthalate has been shown to alter the expression of specific miRNAs (including miR-200a and miR-17) involved in insulin signaling and glucose metabolism,[53] highlighting the regulatory roles of miRNAs in mediating EDC-induced toxicity. These findings align with our observation of 31 differentially expressed miRNAs ($|\log_2$ (fold change)$| > 1$ and $P < 0.05$) associated with 4-tBP-induced hepatotoxicity (Figure 3A). Among them, miR-363 was the most significantly differentially expressed, with its downregulation confirmed both *in vivo* (Figure 3B) and *in vitro* (Figure 3C). MiR-363 has been validated to be involved in regulating inflammation[56] and glycogen metabolism.[57] To explore the role of miR-363 in the 4-tBP-mediated glycogen synthesis disruption, we used insulin, a critical hormone that promotes hepatic glycogen synthesis, as a functional assay to evaluate glycogen synthesis capability.[58] Insulin-stimulated glycogen synthesis was diminished ($P > 0.05$) in cells with miR-363 inhibitor or 4-tBP, while miR-363 mimic reversed ($P < 0.05$) 4-tBP-blunted insulin sensitivity (Figure S4). These findings indicated the pivotal role of miR-363 in restoring glycogen synthesis disrupted by 4-tBP, further highlighting its potential as a therapeutic target for mitigating the hepatotoxic effects of 4-tBP.

3.5. The MiR-363/PKCδ Axis is a Key Modulator in 4-tBP-Induced Inflammatory and Glycogen Metabolism Disruptions

MiRNAs regulate gene expression by binding to the 3′ UTR of target mRNAs, and the miRNA-mRNA axes have been recognized as promising therapeutic targets in various diseases.[59] In this study, PKCδ was identified as a potential miR-363 target due to its predicted binding site (Figure 3D). PKCδ is crucial in inflammatory processes and hepatic glycogen metabolism.[32,60] As a key effector in the NF-κB pathway, PKCδ activation promotes the production of pro-inflammatory cytokines such as IL-1β and IL-6, thereby amplifying inflammatory responses and oxidative stress in diabetic models.[61] Moreover, PKCδ dysregulation has been linked to insulin signaling disruptions, as it contributes to the inhibitory phosphorylation of IRS1 at Ser307, impairing downstream AKT activation and glycogen synthesis.[62,63] Our findings demonstrated that exposure to 4-tBP significantly ($P < 0.05$) upregulated PKCδ mRNA levels in a dose-dependent manner (Figure 3F,G). This upregulation inversely correlates with the downregulation of miR-363 levels, indicating a potential mechanistic interplay between miR-363 and PKCδ under 4-tBP exposure. A dual-luciferase reporter assay further confirmed the specificity of the interaction between miR-363 and the binding site on PKCδ, with a significant ($P < 0.05$) reduction in luciferase activity of PKCδ-WT when treated with miR-363 mimic but no notable change ($P > 0.05$) observed in the mutant group (Figure 3E). Furthermore, miR-363 mimic significantly ($P < 0.05$) decreased both mRNA (Figure 3H) and protein (Figure S5, Uncropped Western blots for Figure S6) levels of PKCδ. In contrast, inhibition of miR-363 caused an increase ($P < 0.05$) in PKCδ expression, which was reversed by siRNA-mediated PKCδ knockdown. These findings revealed the intricate regulatory relationship between miR-

https://doi.org/10.1021/envhealth.4c00242
Environ. Health 2025, 3, 539−550

363 and PKCδ, consistent with specific binding interactions reported in other studies.[64]

It is hypothesized that miR-363 may modulate the inflammatory response and glycogen synthesis by targeting PKCδ. To validate this hypothesis, we investigated the role of the miR-363/PKCδ axis in modulating NF-κB and insulin signaling in hepatocytes exposed to 4-tBP. As depicted in Figure 4A−F, treatment with miR-363 mimic significantly ($P < 0.05$) reduced both mRNA and protein levels associated with NF-κB signaling, indicating a protective role of miR-363 against hepatic inflammation. This aligns with previous research showing that overexpression of miR-363 suppressed pro-inflammatory cytokine expression in dendritic cells of patients with rheumatoid arthritis.[65] These findings highlight the anti-inflammatory potential of miR-363 across different cellular contexts. Additionally, our Western blot analysis (Figure 4G−I, Uncropped Western blots for Figure S6) disclosed that miR-363 mimic effectively ($P < 0.05$) countered the negative effects of 4-tBP on the phosphorylation states of IRS1 and AKT. This counteraction suggested that miR-363 mimics mitigate 4-tBP-induced disruptions in glycogen synthesis by restoring insulin signaling. Conversely, inhibition of miR-363 exacerbated ($P < 0.05$) the effects of 4-tBP on both NF-κB signaling gene expression and the phosphorylation states of IRS1 and AKT. These results highlight miR-363 as a key regulator of inflammatory and insulin signaling networks in response to 4-tBP exposure. Notably, siRNA-mediated PKCδ knockdown provided a balanced modulation, significantly ($P < 0.05$) influencing the effects of miR-363 and alleviating ($P < 0.05$) 4-tBP-induced NF-κB pathway activation and insulin signaling disruption. These findings are supported by recent studies.[61,63] PKCδ induces inflammatory response through the activation of the NF-kB signaling pathway, with its inhibition reducing NF-kB p65, IL-1β, and IL-6 levels in Alzheimer's disease mice.[61] Specific inhibition of PKCδ has also been demonstrated to reverse the increase in p-IRS1 Ser307 and the decrease in p-AKT Ser-473 induced by insulin stimulation, thereby enhancing glycogen synthesis capacity.[63] Together, these findings highlight the miR-363/PKCδ axis as a potential therapeutic target to mitigate the adverse effects of 4-tBP on inflammation and glycogen metabolism (Figure 5).

4. CONCLUSION

In summary, our data demonstrate that chronic exposure to environmentally relevant levels of 4-tBP induces hepatotoxicity in *Cyprinus carpio* L. via impairments in the fish's antioxidant defense capabilities, inflammation induction, and glycogen metabolism disruption. At the molecular level, we demonstrated the key regulatory role of miR-363/PKCδ axis for the hepatoxicity observed in *Cyprinus carpio* L. Exposure to 4-tBP triggers downregulation of miR-363 and upregulation of PKCδ mRNA, disrupting the miR-363/PKCδ axis. This results in (1) increased expression of the NF-κB signaling gene, triggering inflammatory responses, and (2) interfered phosphorylation of IRS1, AKT, and GSK3β, impairing glycogen synthesis. Overexpression of miR-363 or silencing PKCδ mitigated these adverse effects on NF-κB signaling and insulin pathway phosphorylation, highlighting the miR-363/PKCδ axis as a potential therapeutic target against the adverse effects of 4-tBP. Given that miRNA-mRNA axes are recognized as therapeutic targets in various diseases, our study not only sheds light on the molecular mechanisms underlying 4-tBP toxicity and its risks to aquatic organisms but also highlights potential targets for intervention.

■ ASSOCIATED CONTENT

Supporting Information

The Supporting Information is available free of charge at https://pubs.acs.org/doi/10.1021/envhealth.4c00242.

Additional experimental details, materials, methods, and results, including fish culture and treatment, the miRNA-sequencing and target-gene prediction, cell culture experiments, PAS staining, plasmids construction and dual-luciferase reporter assay, Western blot assay, relevant information on sequences and antibodies, and pivotal responses *in vivo* and *in vitro* (PDF)

■ AUTHOR INFORMATION

Corresponding Author

Li Zhou − *Institute of Environmental Research at Greater Bay Area, Key Laboratory for Water Quality and Conservation of the Pearl River Delta, Ministry of Education, Guangzhou University, Guangzhou 510006, China;* orcid.org/0000-0002-8487-4981; Email: zhoul@gzhu.edu.cn

Authors

Jiawen Cui − *Institute of Environmental Research at Greater Bay Area, Key Laboratory for Water Quality and Conservation of the Pearl River Delta, Ministry of Education, Guangzhou University, Guangzhou 510006, China*

Xinchi Shang − *Key Open Laboratory of Cold Water Fish Germplasm Resources and Breeding of Heilongjiang Province, Heilongjiang River Fisheries Research Institute, Chinese Academy of Fishery Sciences, Harbin 150070, China*

Yuhao Liu − *College of Animal Science and Technology, Northeast Agricultural University, Harbin 150030, China*

Xiaohua Teng − *College of Animal Science and Technology, Northeast Agricultural University, Harbin 150030, China*

Bing Yan − *Institute of Environmental Research at Greater Bay Area, Key Laboratory for Water Quality and Conservation of the Pearl River Delta, Ministry of Education, Guangzhou University, Guangzhou 510006, China*

Complete contact information is available at: https://pubs.acs.org/10.1021/envhealth.4c00242

Author Contributions

Jiawen Cui: Conceptualization, Methodology, Software, Formal analysis, Data Curation, Writing - Original Draft, Validation. **Xinchi Shang:** Methodology, Investigation, Data Curation. **Yuhao Liu:** Methodology, Software. **Xiaohua Teng:** Supervision, Conceptualization, Data Curation. **Li Zhou:** Methodology, Software, Writing-Review & Editing. **Bing Yan:** Supervision, Funding acquisition, Writing-Review & Editing.

Notes

The authors declare no competing financial interest.

■ ACKNOWLEDGMENTS

This work was supported by the National Natural Science Foundation of China (22376042 and 21906033), the introduced innovative R&D team project under the "The Pearl River Talent Recruitment Program" of Guangdong

Province (2019ZT08L387), and Science and Technology Projects of Guangzhou (202201020392) and Science and Technology Development Plan Project of Jilin (YDZJ202201-ZYTS692).

REFERENCES

(1) Janousek, R. M.; Müller, J.; Knepper, T. P. Combined study of source, environmental monitoring and fate of branched alkylphenols: The chain length matters. *Chemosphere* **2020**, *241*, 124950.
(2) Park, S. R.; Park, S. J.; Jeong, M. J.; Choi, J. C.; Kim, M. Fast and simple determination and exposure assessment of bisphenol A, phenol, p-tert-butylphenol, and diphenylcarbonate transferred from polycarbonate food-contact materials to food simulants. *Chemosphere* **2018**, *203*, 300−306.
(3) Tang, P.; Shu, J.; Xie, W.; Su, Y.; He, Q.; Liu, B. Characterizing hazardous substances of shale gas wastewater from the upper Yangtze River: A focus on heavy metals and organic compounds. *Journal of hazardous materials* **2024**, *469*, 133873.
(4) Bell, A. M.; Baier, R.; Kocher, B.; Reifferscheid, G.; Buchinger, S.; Ternes, T. Ecotoxicological characterization of emissions from steel coatings in contact with water. *Water Res.* **2020**, *173*, 115525.
(5) Liu, Y. H.; Zhang, S. H.; Ji, G. X.; Wu, S. M.; Guo, R. X.; Cheng, J.; Yan, Z. Y.; Chen, J. Q. Occurrence, distribution and risk assessment of suspected endocrine-disrupting chemicals in surface water and suspended particulate matter of Yangtze River (Nanjing section). *Ecotoxicology and environmental safety* **2017**, *135*, 90−97.
(6) Kurata, Y.; Ono, Y.; Ono, Y. Occurrence of phenols in leachates from municipal solid waste landfill sites in Japan. *Journal of Material Cycles and Waste Management* **2008**, *10* (2), 144−152.
(7) Ko, E. J.; Kim, K. W.; Kang, S. Y.; Kim, S. D.; Bang, S. B.; Hamm, S. Y.; Kim, D. W. Monitoring of environmental phenolic endocrine disrupting compounds in treatment effluents and river waters, Korea. *Talanta* **2007**, *73* (4), 674−83.
(8) OECD SIDS *p-tert-Butylphenol, SIDS Initial Assessment Report for 10th SIAM*; UNEP Publications, 2000.
(9) Haavisto, T. E.; Adamsson, N. A.; Myllymäki, S. A.; Toppari, J.; Paranko, J. Effects of 4-tert-octylphenol, 4-tert-butylphenol, and diethylstilbestrol on prenatal testosterone surge in the rat. *Reproductive toxicology (Elmsford, N.Y.)* **2003**, *17* (5), 593−605.
(10) Wang, H.; Liu, J.; Qiang, S.; Che, Y.; Hu, T. 4-tert-Butylphenol impairs the liver by inducing excess liver lipid accumulation via disrupting the lipid metabolism pathway in zebrafish. *Environ. Pollut.* **2024**, *356*, 124385.
(11) Wang, M.; Qin, T.; Chen, G.; Wang, G.; Hu, T. The toxicity of 4-tert-butylphenol in early development of zebrafish: morphological abnormality, cardiotoxicity, and hypopigmentation. *Environmental science and pollution research international* **2023**, *30* (16), 45781−45795.
(12) Barse, A. V.; Chakrabarti, T.; Ghosh, T. K.; Pal, A. K.; Jadhao, S. B. One-tenth dose of LC50 of 4-tert-butylphenol causes endocrine disruption and metabolic changes in Cyprinus carpio. *Pesticide Biochemistry & Physiology* **2006**, *86* (3), 172−179.
(13) Pastor-Belda, M.; Drauschke, T.; Campillo, N.; Arroyo-Manzanares, N.; Torres, C.; Pérez-Cárceles, M. D.; Hernández-Córdoba, M.; Viñas, P. Dual stir bar sorptive extraction coupled to thermal desorption-gas chromatography-mass spectrometry for the determination of endocrine disruptors in human tissues. *Talanta* **2020**, *207*, 120331.
(14) Sundt, R. C.; Baussant, T.; Beyer, J. Uptake and tissue distribution of C4-C7 alkylphenols in Atlantic cod (Gadus morhua): relevance for biomonitoring of produced water discharges from oil production. *Marine pollution bulletin* **2009**, *58* (1), 72−9.
(15) Cui, J.; Zhou, Q.; Yu, M.; Liu, Y.; Teng, X.; Gu, X. 4-tert-butylphenol triggers common carp hepatocytes ferroptosis via oxidative stress, iron overload, SLC7A11/GSH/GPX4 axis, and ATF4/HSPA5/GPX4 axis. *Ecotoxicology and environmental safety* **2022**, *242*, 113944.
(16) Liu, M.; Dong, F.; Yi, S.; Zhu, Y.; Zhou, J.; Sun, B.; Shan, G.; Feng, J.; Zhu, L. Probing Mechanisms for the Tissue-Specific Distribution and Biotransformation of Perfluoroalkyl Phosphinic Acids in Common Carp (Cyprinus carpio). *Environ. Sci. Technol.* **2020**, *54* (8), 4932−4941.
(17) Song, P.; Jiang, N.; Zhang, K.; Li, X.; Li, N.; Zhang, Y.; Wang, Q.; Wang, J. Ecotoxicological evaluation of zebrafish liver (Danio rerio) induced by dibutyl phthalate. *Journal of hazardous materials* **2022**, *425*, 128027.
(18) Song, P.; Jiang, N.; Zhang, K.; Li, X.; Li, N.; Zhang, Y.; Wang, Q.; Wang, J. Ecotoxicological evaluation of zebrafish liver (Danio rerio) induced by dibutyl phthalate. *J. Hazard. Mater.* **2022**, *425*, 128027.
(19) Sanchez, W.; Burgeot, T.; Porcher, J. M. A novel "Integrated Biomarker Response" calculation based on reference deviation concept. *Environmental science and pollution research international* **2013**, *20* (5), 2721−5.
(20) Cui, J.; Liu, Y.; Hao, Z.; Liu, Y.; Qiu, M.; Kang, L.; Teng, X.; Tang, Y. Cadmium induced time-dependent kidney injury in common carp via mitochondrial pathway: Impaired mitochondrial energy metabolism and mitochondrion-dependent apoptosis. *Aquat Toxicol* **2023**, *261*, 106570.
(21) Wang, Y.; Liu, Z.; Ma, J.; Xv, Q.; Gao, H.; Yin, H.; Yan, G.; Jiang, X.; Yu, W. Lycopene attenuates the inflammation and apoptosis in aristolochic acid nephropathy by targeting the Nrf2 antioxidant system. *Redox biology* **2022**, *57*, 102494.
(22) Chen, J.; Zhang, S.; Tong, J.; Teng, X.; Zhang, Z.; Li, S.; Teng, X. Whole transcriptome-based miRNA-mRNA network analysis revealed the mechanism of inflammation-immunosuppressive damage caused by cadmium in common carp spleens. *Science of The Total Environment* **2020**, *717*, 137081.
(23) Katikaneni, A.; Jelcic, M.; Gerlach, G. F.; Ma, Y.; Overholtzer, M.; Niethammer, P. Lipid peroxidation regulates long-range wound detection through 5-lipoxygenase in zebrafish. *Nature cell biology* **2020**, *22* (9), 1049−1055.
(24) Chen, K.; Wang, Y.; Yang, J.; Klöting, N.; Liu, C.; Dai, J.; Jin, S.; Chen, L.; Liu, S.; Liu, Y.; Yu, Y.; Liu, X.; Miao, Q.; Liew, C. W.; Wang, Y.; Dietrich, A.; Blüher, M.; Wang, X. EMC10 modulates hepatic ER stress and steatosis in an isoform specific manner. *Journal of hepatology* **2024**, *81*, 479.
(25) Guedegba, N. L.; Imorou Toko, I.; Ben Ammar, I.; François, L.; Oreins, N.; Palluel, O.; Mandiki, S. N. M.; Jauniaux, T.; Porcher, J. M.; Scippo, M. L.; Kestemont, P. Chronic effects of a binary insecticide Acer 35 EC on Nile tilapia Oreochromis niloticus through a multi-biomarker approach. *Chemosphere* **2021**, *273*, 128530.
(26) Briaudeau, T.; Alves Dos Santos, L. A.; Zorita, I.; Izagirre, U.; Marigómez, I. Biological responses and toxicopathic effects elicited in Solea senegalensis juveniles by waterborne exposure to benzo[a]-pyrene. *Marine environmental research* **2021**, *170*, 105351.
(27) Yang, H.; Jiang, Y.; Lu, K.; Xiong, H.; Zhang, Y.; Wei, W. Herbicide atrazine exposure induce oxidative stress, immune dysfunction and WSSV proliferation in red swamp crayfish Procambarus clarkii. *Chemosphere* **2021**, *283*, 131227.
(28) Cai, H.; Li, K.; Yin, Y.; Ni, X.; Xu, S. Quercetin alleviates DEHP exposure-induced pyroptosis and cytokine expression changes in grass carp L8824 cell line by inhibiting ROS/MAPK/NF-κB pathway. *Fish & shellfish immunology* **2023**, *143*, 109223.
(29) Li, S.; Gu, X.; Zhang, M.; Jiang, Q.; Xu, T. Di (2-ethylhexyl) phthalate and polystyrene microplastics co-exposure caused oxidative stress to activate NF-κB/NLRP3 pathway aggravated pyroptosis and inflammation in mouse kidney. *Science of the total environment* **2024**, *926*, 171817.
(30) Ziegler, K.; Kunert, A. T.; Reinmuth-Selzle, K.; Leifke, A. L.; Widera, D.; Weller, M. G.; Schuppan, D.; Fröhlich-Nowoisky, J.; Lucas, K.; Pöschl, U. Chemical modification of pro-inflammatory proteins by peroxynitrite increases activation of TLR4 and NF-κB: Implications for the health effects of air pollution and oxidative stress. *Redox biology* **2020**, *37*, 101581.

(31) Fu, J.; Schroder, K.; Wu, H. Mechanistic insights from inflammasome structures. *Nature Reviews Immunology* **2024**, *24* (7), 518−535.
(32) Zhang, L.; Wang, W.; Chen, T.; Cui, J.; Li, X.; Liu, A.; Liu, R.; Fang, L.; Jiang, J.; Yang, L.; Wu, D.; Ying, S. SAMHD1 dysfunction induces IL-34 expression via NF-κB p65 in neuronal SH-SY5Y cells. *Molecular immunology* **2024**, *168*, 1−9.
(33) Candellier, A.; Issa, N.; Grissi, M.; Brouette, T.; Avondo, C.; Gomila, C.; Blot, G.; Gubler, B.; Touati, G.; Bennis, Y.; Caus, T.; Brazier, M.; Choukroun, G.; Tribouilloy, C.; Kamel, S.; Boudot, C.; Hénaut, L. Indoxyl-sulfate activation of the AhR- NF-κB pathway promotes interleukin-6 secretion and the subsequent osteogenic differentiation of human valvular interstitial cells from the aortic valve. *Journal of molecular and cellular cardiology* **2023**, *179*, 18−29.
(34) Kao, M. H.; Wu, J. S.; Cheung, W. M.; Chen, J. J.; Sun, G. Y.; Ong, W. Y.; Herr, D. R.; Lin, T. N. Clinacanthus nutans Mitigates Neuronal Death and Reduces Ischemic Brain Injury: Role of NF-κB-driven IL-1β Transcription. *Neuromolecular medicine* **2021**, *23* (1), 199−210.
(35) Sun, Q.; Liu, Y.; Teng, X.; Luan, P.; Teng, X.; Yin, X. Immunosuppression participated in complement activation-mediated inflammatory injury caused by 4-octylphenol via TLR7/IκBα/NF-κB pathway in common carp (Cyprinus carpio) gills. *Aquatic toxicology (Amsterdam, Netherlands)* **2022**, *249*, 106211.
(36) Yu, J.; Tuo, F.; Luo, Y.; Yang, Y.; Xu, J. Toxic effects of perinatal maternal exposure to nonylphenol on lung inflammation in male offspring rats. *Science of the total environment* **2020**, *737*, 139238.
(37) Ainiwaer, P.; Li, Z.; Zang, D.; Jiang, L.; Zou, G.; Aisa, H. A. Ruta graveolens: Boost Melanogenic Effects and Protection against Oxidative Damage in Melanocytes. *Antioxidants (Basel, Switzerland)* **2023**, *12* (8), 1580.
(38) Wang, H.; Liu, J.; Qiang, S.; Che, Y.; Hu, T. 4-tert-Butylphenol impairs the liver by inducing excess liver lipid accumulation via disrupting the lipid metabolism pathway in zebrafish. *Environmental pollution (Barking, Essex: 1987)* **2024**, *356*, 124385.
(39) Zhou, H.; Wang, H.; Yu, M.; Schugar, R. C.; Qian, W.; Tang, F.; Liu, W.; Yang, H.; McDowell, R. E.; Zhao, J.; Gao, J.; Dongre, A.; Carman, J. A.; Yin, M.; Drazba, J. A.; Dent, R.; Hine, C.; Chen, Y.-R.; Smith, J. D.; Fox, P. L.; Brown, J. M.; Li, X. IL-1 induces mitochondrial translocation of IRAK2 to suppress oxidative metabolism in adipocytes. *Nature Immunology* **2020**, *21* (10), 1219−1231.
(40) Heo, Y. J.; Choi, S. E.; Jeon, J. Y.; Han, S. J.; Kim, D. J.; Kang, Y.; Lee, K. W.; Kim, H. J. Visfatin Induces Inflammation and Insulin Resistance via the NF-κB and STAT3 Signaling Pathways in Hepatocytes. *Journal of diabetes research* **2019**, *2019*, 4021623.
(41) Guo, X.; Pu, J.; Tang, Z.; Jia, C.; Yang, F.; Liu, T.; Ding, Y. LRP1 facilitates hepatic glycogenesis by improving the insulin signaling pathway in HFD-fed mice. *Animal models and experimental medicine* **2024**, *7*, 696.
(42) Xu, E.; Pereira, M. M. A.; Karakasilioti, I.; Theurich, S.; Al-Maarri, M.; Rappl, G.; Waisman, A.; Wunderlich, F. T.; Brüning, J. C. Temporal and tissue-specific requirements for T-lymphocyte IL-6 signalling in obesity-associated inflammation and insulin resistance. *Nat. Commun.* **2017**, *8* (1), 14803.
(43) Jing, H.; Gao, X.; Xu, L.; Lin, H.; Zhang, Z. H2S promotes a glycometabolism disorder by disturbing the Th1/Th2 balance during LPS-induced inflammation in the skeletal muscles of chickens. *Chemosphere* **2019**, *222*, 124−131.
(44) Jacob Berger, A.; Gigi, E.; Kupershmidt, L.; Meir, Z.; Gavert, N.; Zwang, Y.; Prior, A.; Gilad, S.; Harush, U.; Haviv, I.; Stemmer, S. M.; Blum, G.; Merquiol, E.; Mardamshina, M.; Kaminski Strauss, S.; Friedlander, G.; Bar, J.; Kamer, I.; Reizel, Y.; Geiger, T.; Pilpel, Y.; Levin, Y.; Tanay, A.; Barzel, B.; Reuveni, H.; Straussman, R. IRS1 phosphorylation underlies the non-stochastic probability of cancer cells to persist during EGFR inhibition therapy. *Nature Cancer* **2021**, *2* (10), 1055−1070.
(45) Woo, J. R.; Bae, S. H.; Wales, T. E.; Engen, J. R.; Lee, J.; Jang, H.; Park, S. The serine phosphorylations in the IRS-1 PIR domain abrogate IRS-1 and IR interaction. *Proc. Natl. Acad. Sci. U.S.A.* **2024**, *121* (17), No. e2401716121.
(46) Ruiz-Alcaraz, A. J.; Liu, H. K.; Cuthbertson, D. J.; McManus, E. J.; Akhtar, S.; Lipina, C.; Morris, A. D.; Petrie, J. R.; Hundal, H. S.; Sutherland, C. A novel regulation of IRS1 (insulin receptor substrate-1) expression following short term insulin administration. *Biochemical journal* **2005**, *392* (2), 345−52.
(47) Hwang, J.-H.; Kim, A. R.; Kim, K. M.; Il Park, J.; Oh, H. T.; Moon, S. A.; Byun, M. R.; Jeong, H.; Kim, H. K.; Yaffe, M. B.; Hwang, E. S.; Hong, J.-H. TAZ couples Hippo/Wnt signalling and insulin sensitivity through Irs1 expression. *Nat. Commun.* **2019**, *10* (1), 421.
(48) Liao, S.; Wu, J.; Liu, R.; Wang, S.; Luo, J.; Yang, Y.; Qin, Y.; Li, T.; Zheng, X.; Song, J.; Zhao, X.; Xiao, C.; Zhang, Y.; Bian, L.; Jia, P.; Bai, Y.; Zheng, X. A novel compound DBZ ameliorates neuroinflammation in LPS-stimulated microglia and ischemic stroke rats: Role of Akt(Ser473)/GSK3β(Ser9)-mediated Nrf2 activation. *Redox biology* **2020**, *36*, 101644.
(49) Du, Y.; Zhou, Y.; Yan, X.; Pan, F.; He, L.; Guo, Z.; Hu, Z. APE1 inhibition enhances ferroptotic cell death and contributes to hepatocellular carcinoma therapy. *Cell Death & Differentiation* **2024**, *31* (4), 431−446.
(50) Wang, H.; Lei, X.; Zhang, Z.; Ommati, M. M.; Tang, Z.; Yuan, J. Chronic exposure of bisphenol-A impairs cognitive function and disrupts hippocampal insulin signaling pathway in male mice. *Toxicology* **2022**, *472*, 153192.
(51) Parsanathan, R.; Maria Joseph, A.; Karundevi, B. Postnatal exposure to di-(2-ethylhexyl)phthalate alters cardiac insulin signaling molecules and GLUT4(Ser488) phosphorylation in male rat offspring. *Journal of cellular biochemistry* **2019**, *120* (4), 5802−5812.
(52) Pan, Y.; Shan, D.; Ding, L.-l.; Yang, X.-d.; Xu, K.; Huang, H.; Wang, J.-f.; Ren, H.-q. Developing a generally applicable electrochemical sensor for detecting macrolides in water with thiophene-based molecularly imprinted polymers. *Water Res.* **2021**, *205*, 117670.
(53) Wei, J.; Hao, Q.; Chen, C.; Li, J.; Han, X.; Lei, Z.; Wang, T.; Wang, Y.; You, X.; Chen, X.; Li, H.; Ding, Y.; Huang, W.; Hu, Y.; Lin, S.; Shen, H.; Lin, Y. Epigenetic repression of miR-17 contributed to di(2-ethylhexyl) phthalate-triggered insulin resistance by targeting Keap1-Nrf2/miR-200a axis in skeletal muscle. *Theranostics* **2020**, *10* (20), 9230−9248.
(54) Cui, J.; Liang, Z.; Liu, Y.; Hao, Z.; Tang, Y.; Zhou, L.; Teng, X. Environmental endocrine disrupting chemical 4-tert-butylphenol induced calcium overload and subsequent autophagy impairment via miRNA-363/CACNA1D Axis in epithelioma papulosum cyprini cells. *Comparative biochemistry and physiology. Toxicology & pharmacology: CBP* **2024**, *283*, 109968.
(55) Kim, J. H.; Cho, Y. H.; Hong, Y.-C. MicroRNA expression in response to bisphenol A is associated with high blood pressure. *Environ. Int.* **2020**, *141*, 105791.
(56) Carvalho, G. B.; Brandão-Lima, P. N.; Payolla, T. B.; Lucena, S. E. F.; Sarti, F. M.; Fisberg, R. M.; Rogero, M. M. Circulating MiRNAs Are Associated With Low-grade Systemic Inflammation and Leptin Levels in Older Adults. *Inflammation* **2023**, *46* (6), 2132−2146.
(57) Peng, Y. H.; Wang, P.; He, X. Q.; Hong, M. Z.; Liu, F. Micro ribonucleic acid-363 regulates the phosphatidylinositol 3-kinase/threonine protein kinase axis by targeting NOTCH1 and forkhead box C2, leading to hepatic glucose and lipids metabolism disorder in type 2 diabetes mellitus. *Journal of diabetes investigation* **2022**, *13* (2), 236−248.
(58) De Toni, L.; Di Nisio, A.; Rocca, M. S.; Guidolin, D.; Della Marina, A.; Bertazza, L.; Sut, S.; Purpura, E.; Pannella, M.; Garolla, A.; Foresta, C. Exposure to Perfluoro-Octanoic Acid Associated With Upstream Uncoupling of the Insulin Signaling in Human Hepatocyte Cell Line. *Front Endocrinol (Lausanne)* **2021**, *12*, 632927.
(59) Hennig, T.; Prusty, A. B.; Kaufer, B. B.; Whisnant, A. W.; Lodha, M.; Enders, A.; Thomas, J.; Kasimir, F.; Grothey, A.; Klein, T.; Herb, S.; Jürges, C.; Sauer, M.; Fischer, U.; Rudel, T.; Meister, G.; Erhard, F.; Dölken, L.; Prusty, B. K. Selective inhibition of miRNA processing by a herpesvirus-encoded miRNA. *Nature* **2022**, *605* (7910), 539−544.

https://doi.org/10.1021/envhealth.4c00242
Environ. Health 2025, 3, 539−550

(60) Ghoshal, K.; Luther, J. M.; Pakala, S. B.; Chetyrkin, S.; Falck, J. R.; Zent, R.; Wasserman, D. H.; Pozzi, A. Epoxygenase Cyp2c44 Regulates Hepatic Lipid Metabolism and Insulin Signaling by Controlling FATP2 Localization and Activation of the DAG/PKCδ Axis. *Diabetes* **2024**, *73* (8), 1229−1243.
(61) Du, Y.; Guo, T.; Hao, Y.; Li, C.; Tang, L.; Li, X.; Zhang, X.; Li, L.; Yao, D.; Xu, X.; Si, H.; Zhang, J.; Zhao, N.; Yu, T.; Zhao, Y.; Zhang, W.; Xu, H. PKCδ serves as a potential biomarker and therapeutic target for microglia-mediated neuroinflammation in Alzheimer's disease. *Alzheimer's & dementia: the journal of the Alzheimer's Association* **2024**, *20* (8), 5511−5527.
(62) Khamaisi, M.; Katagiri, S.; Keenan, H.; Park, K.; Maeda, Y.; Li, Q.; Qi, W.; Thomou, T.; Eschuk, D.; Tellechea, A.; Veves, A.; Huang, C.; Orgill, D. P.; Wagers, A.; King, G. L. PKCδ inhibition normalizes the wound-healing capacity of diabetic human fibroblasts. *J. Clin. Invest.* **2016**, *126* (3), 837−53.
(63) Greene, M. W.; Ruhoff, M. S.; Burrington, C. M.; Garofalo, R. S.; Oreña, S. J. TNFalpha activation of PKCdelta, mediated by NFkappaB and ER stress, cross-talks with the insulin signaling cascade. *Cellular signalling* **2010**, *22* (2), 274−84.
(64) Miao, Z.; Miao, Z.; Teng, X.; Xu, S. Chlorpyrifos triggers epithelioma papulosum cyprini cell pyroptosis via miR-124−3p/CAPN1 axis. *Journal of hazardous materials* **2022**, *424* (Pt A), 127318.
(65) Pan, F.; Xiang, H.; Yan, J.; Hong, L.; Zhang, L.; Liu, Y.; Feng, X.; Cai, C. Dendritic Cells from Rheumatoid Arthritis Patient Peripheral Blood Induce Th17 Cell Differentiation via miR-363/Integrin αv/TGF-β Axis. *Scandinavian journal of immunology* **2017**, *85* (6), 441−449.

https://doi.org/10.1021/envhealth.4c00242
Environ. Health 2025, 3, 539−550